J. Fluid Mech. (1999), *vol.* 398, *pp.* 87–108. Printed in the United Kingdom

Nonlinear stability of mixed convection flow under non-Boussinesq conditions. Part 2. Mean flow characteristics

By S. A. SUSLOV† AND S. PAOLUCCI

Department of Aerospace and Mechanical Engineering, University of Notre Dame, Notre Dame, IN 46556, USA

(Received 10 January 1998 and in revised form 26 May 1999)

Based on amplitude expansions developed in Part 1 (Suslov & Paolucci 1999), we examine the mean flow characteristics of non-Boussinesq mixed convection flow of air in a vertical channel in the vicinity of bifurcation points for a wide range of temperature differences between the walls, and Grashof and Reynolds numbers. The constant mass flux and constant pressure gradient formulations are shown to lead to qualitatively similar, but quantitatively different, results. The physical nature of the distinct shear and buoyancy disturbances is investigated, and detailed mean flow and energy analyses are presented. The variation of the total mass of fluid in a flow domain as disturbances develop is discussed. The average Nusselt number and mass flux are estimated for supercritical regimes for a wide range of governing parameters.

1. Introduction

Convection plays a significant role in many technical applications. Frequently, it defines the major mechanism for heat and mass transfer in fluids. It was shown recently in Suslov & Paolucci (1995*a*, *b*, 1997*b*) that the fluid property variations within the domain can lead to flows substantially different from those predicted based on models such as the conventional Boussinesq approximation of the Navier–Stokes equations. Most commonly, significant fluid property variations are caused by large temperature gradients between different regions within the flow. Indeed such a situation typically occurs, for example, in heat exchangers, chemical vapour deposition reactors, and thermal insulation systems of nuclear reactors. The characteristic temperature difference in such applications is comparable with the average temperature of the fluid. Naturally, variations of fluid density, viscosity and thermal conductivity cannot be neglected in such conditions.

In our earlier works (Suslov & Paolucci 1995*a*, *b*) we have undertaken a linear analysis of such flows with respect to periodic disturbances and investigated the effect of fluid property variations on the stability of a parallel shear flow in a conduction state. In particular, the boundary of instability as well as spatial eigenfunctions which define the form of periodic disturbances were computed. While linear analysis is useful to obtain qualitative characteristics of resulting unstable flows, it does not provide quantitative information on the actual size of the disturbances. For this, nonlinear analysis is necessary.

† Current Address: Department of Mathematics and Computing, University of Southern Queensland, Toowoomba, Queensland 4350, Australia.

Typically, weakly nonlinear analysis is based on an asymptotic expansion. The amplitude of disturbances is a convenient and frequently preferred choice of the small parameter for such an expansion (see, for example, discussions in Watson 1960; Herbert 1983; Suslov & Paolucci 1997*b*). Then the solution to the problem is sought in the form

$$u = u_{00}(x) + [A(t)u_{11}(x)\exp(\mathrm{i}\alpha y) + \text{c.c.}] + |A(t)|^2 u_{20}(x) + \cdots, \tag{1}$$

where c.c. denotes the complex conjugate of the preceding expression within the brackets (see Part 1, Suslov & Paolucci 1999). The above equation assumes that the bifurcation of a steady one-dimensional basic state $u_{00}(x)$ into an unsteady two-dimensional periodic state is being investigated. The general derivation of the form of such an expansion is given in Suslov & Paolucci (1997*b*) for the flow of a fluid with arbitrary property variations and generalized for the flow of such a fluid in open systems in Part 1. Generally, one is primarily interested in the leading-order term of the equilibrium state attained after the bifurcation. This state is characterized by the equilibrium amplitude A_e and by the eigenfunction $u_{11}(x)$ of the linear problem. The equilibrium amplitude corresponds to a fixed point of the Landau equation which governs the time evolution of the disturbance amplitude (see Part 1). The derivation of the Landau equation requires knowledge of the mean flow correction $u_{20}(x)$ and other second-order terms which arise in expansion (1). Thus, on the surface, it appears that the mean flow correction just plays a passive role in weakly nonlinear analysis. This is not so because even if both the equilibrium amplitude and the eigenfunction of the linear problem are known, they do not provide any information on integral characteristics of the flow past bifurcation since the contribution of the leading term of the disturbance to the mean motion is zero owing to the spatial (and possibly temporal) periodicity. Thus, such important characteristics of the flow as the mean flow rate and heat flux as well as the energy balance cannot be determined solely by the leading-order approximation of the disturbance. One has to consider second-order correction terms to remove this limitation. The deficiency of the leading-order approximation becomes even more of a problem when one has to analyse the selection between several instability modes which are driven by different physical mechanisms, and which become equally important in the vicinity of codimensional points where a number of critical modes compete with each other (Suslov & Paolucci 1997*a*). As shown in Suslov & Paolucci (1995*b*), competition between the different modes of instability in non-Boussinesq mixed convection flow is found for multiple values in the governing parameters space. The present paper aims to extend the discussion of the modes obtained in Suslov & Paolucci (1995*b*) by considering the mean flow corrections arising from these modes.

Note that, in contrast to the Boussinesq case, under non-Boussinesq conditions the density of the fluid changes with time. This means that in general the total mass of the fluid in the system changes. Such a situation requires a special treatment in the weakly nonlinear analysis which is addressed in Part 1. In this paper we provide numerical results characterizing this change of the total mass of fluid in a channel.

This work is organized as follows. First, the problem is formulated for two physically distinct cases of fluid flow within a channel: fixed average longitudinal pressure gradient and fixed average mass flux. Next, the expansion procedure is outlined and properties of the resulting system of equations are discussed. Finally, the theory is applied to the non-Boussinesq mixed convection flow of air in a vertical channel. Results are given for a wide range of temperature differences between the walls, and Grashof and Reynolds numbers.

2. Problem definition and governing equations

A two-dimensional mixed convection flow between two vertical infinite isothermal plates separated by a distance H and maintained at the temperature difference $\Delta T = T_h^* - T_c^*$ is governed by the low-Mach-number equations (Paolucci 1992) written in non-dimensional form as

$$\frac{\partial}{\partial t}(\rho u_i) + \frac{\partial}{\partial x_j}(\rho u_i u_j) = -\frac{\partial \Pi}{\partial x_i} + \frac{Gr}{2\epsilon}(\rho - 1)n_i + \frac{\partial \tau_{ij}}{\partial x_j}, \tag{2}$$

$$\rho c_p \left(\frac{\partial T}{\partial t} + u_j \frac{\partial T}{\partial x_j}\right) = \frac{1}{Pr}\frac{\partial}{\partial x_j}\left(k\frac{\partial T}{\partial x_j}\right), \tag{3}$$

$$\frac{\partial \rho}{\partial t} + \frac{\partial \rho u_j}{\partial x_j} = 0, \tag{4}$$

where

$$\tau_{ij} = \mu\left[\left(\frac{\partial u_i}{\partial x_j} + \frac{\partial u_j}{\partial x_i}\right) - \frac{2}{3}\delta_{ij}\frac{\partial u_k}{\partial x_k}\right]. \tag{5}$$

The boundary conditions for the problem are

$$u = v = 0 \quad \text{and} \quad T = 1 \pm \epsilon \quad \text{at} \quad x = 0, 1. \tag{6}$$

The reader is referred to Part 1 for more details.

The dimensionless parameters appearing in the equations are the Grashof number, the dimensionless temperature difference, and the Prandtl number:

$$Gr = \frac{\rho_r^2 \beta_r g \Delta T H^3}{\mu_r^2}, \quad \epsilon = \tfrac{1}{2}\beta_r \Delta T, \quad Pr = \frac{\mu_r c_{pr}}{k_r}, \tag{7}$$

where β_r is the coefficient of thermal expansion evaluated at the reference temperature. As discussed in Part 1 the Reynolds number

$$Re = \frac{\rho_r U_r H}{\mu_r} \tag{8}$$

is associated with the characteristic longitudinal velocity induced by the imposed pressure gradient $\hat{\Pi}^*$

$$U_r = -\frac{H^2}{12\mu_r}\hat{\Pi}^*, \tag{9}$$

when the constant pressure gradient case is considered, or with the mass flux $\dot{m}^*$

$$U_r = \frac{\dot{m}^*}{\rho_r H} = \frac{\overline{\rho^* v^*}}{\rho_r H}, \tag{10}$$

when the mass flux is fixed. Generally, in non-Boussinesq flow the two definitions of U_r lead to two different definitions of the Reynolds numbers. This difference will be discussed further in the paper.

3. Expansions and mean flow equations

We assume that a small-amplitude periodic disturbance is superimposed on a fully developed basic flow, which is stationary and does not depend on the longitudinal coordinate. We then look for the solution of the problem (1)–(6) in the separable

Fourier-decomposed form

$$\boldsymbol{W}(t,x,y) = \boldsymbol{w}_{00} + [A(t)\boldsymbol{w}_{11}E(y) + \text{c.c.}] + |A(t)|^2\boldsymbol{w}_{20} + \cdots, \tag{11}$$

$$\boldsymbol{g}(t,x,y) = \boldsymbol{g}_{00}(x) + [A(t)\,\boldsymbol{g}_{11}(x)\,E(y) + \text{c.c.}] + |A(t)|^2\boldsymbol{g}_{20}(x) + \cdots, \tag{12}$$

where $\boldsymbol{w}_{mn} = (u_{mn}(x),\ v_{mn}(x),\ T_{mn}(x),\ \Pi_{mn}(x)+\delta_{0n}\hat{\Pi}_{m0}y)^T$, $\boldsymbol{g}_{mn}(x)$ are components of the expansion of the property vector $\boldsymbol{g} = (\rho, c_p, \mu, k)^T$, $E = \exp(\mathrm{i}\alpha y)$ is a Fourier component of the disturbance corresponding to a wavenumber α, the first subscript corresponds to the order of small disturbance amplitude $A(t)$ and the second subscript denotes the order of the Fourier exponent. The terms $\hat{\Pi}_{m0}y$ in the expansion for the dynamic pressure are necessary in order to take into account the constant vertical pressure gradient required to maintain a fixed average mass flux through the channel when disturbances are developing. In the case of a fixed longitudinal pressure gradient, $\hat{\Pi}_{m0} = 0$ for $m > 0$. In (11) other quadratic and higher-order terms are not written out since they do not affect the discussion in this work (see Part 1 for the complete expansion). As shown in Part 1 the evolution of the disturbance amplitude up to the third order is given by the Landau equation

$$\frac{\partial|A|^2}{\partial t} = 2|A|\left(\sigma^R + K^R|A|^2\right), \tag{13}$$

where σ^R is the linear amplification rate (Suslov & Paolucci 1995*b*) and K^R is the real part of the Landau constant which has been evaluated for the complete parameter space considered in Part 1. If $K^R < 0$ (supercritical bifurcation) the stable equilibrium value of the amplitude is given by $|A_e|^2 = -\sigma^R/K^R$ for $\sigma^R > 0$ (note that $|A_e| = 0$ for $\sigma^R \leqslant 0$ in this case). Estimation of the stable equilibrium amplitude in case of subcritical bifurcation $K^R > 0$ is much more involved and requires retaining at least fifth-order terms in equation (13). This has not been done in the current work and thus numerical results for the mean flow corrections will be reported only for regions of supercritical bifurcations.

Substituting expansions (11) and (12) into system (1)–(6) we obtain a set of equations at each order of amplitude A and Fourier component E. Here we consider only solutions of the equations arising at $|A|^2E^0$ order. They can be written in vector form as

$$\left(|A|^2\boldsymbol{A}_0 + \frac{\partial|A|^2}{\partial t_0}\boldsymbol{B}\right)\boldsymbol{w}_{20} = |A|^2\boldsymbol{F}_{20}, \tag{14}$$

where $\boldsymbol{w}_{20} = (u_{20},\ v_{20},\ T_{20},\ \Pi_{20})^T$, $u_{20} = v_{20} = T_{20} = 0$ at $x = 0,\ 1$ and the linear matrix operators $\boldsymbol{A}_0$ and $\boldsymbol{B}$ are defined in Part 1. The right-hand-side vector $\boldsymbol{F}_{20} = \boldsymbol{f}_{20} - 2\sigma^R S_\rho \boldsymbol{f}_{20}$, where $\boldsymbol{f}_{20} = (f_{20}^{(1)},\ f_{20}^{(2)},\ f_{20}^{(3)},\ f_{20}^{(4)})^T$ represents quadratic self-interaction of the fundamental harmonic of the disturbance wave and is given in Part 1 and $\boldsymbol{f}_{20} = (u_{00},\ v_{00},\ c_{p00}T_{00},\ 1)^T$. The second term in the expression for $\boldsymbol{F}_{20}$ accounts for the average momentum and thermal energy variation associated with the total fluid mass change in a channel as disturbances develop (the overbar denotes integration over the channel width)

$$S_{\rho 20} = -\overline{\rho_{20}} = \frac{M_0 - M(t)}{|A(t)|^2\lambda} + O(|A(t)|). \tag{15}$$

Introduction of these terms is justified in Part 1. Equation (14) describes the lowest-order mean flow correction associated with the finite-amplitude periodic disturbance wave.

The mean flow correction equation must be treated differently for the two physically

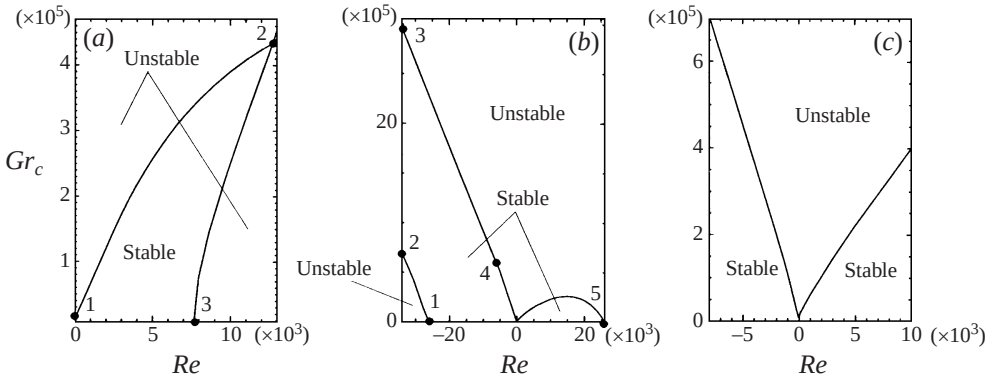

FIGURE 1. Linear stability diagrams for (*a*) $\epsilon = 0.005$, (*b*) $\epsilon = 0.3$, and (*c*) $\epsilon = 0.6$. Labelled points are used in the discussion of figures 4–9.

different situations corresponding to fixed average vertical pressure gradient and fixed average mass flux. In the first case we have $\hat{\Pi}_{20} = 0$, while in the second case we generally have a non-zero pressure gradient $\hat{\Pi}_{20}$, the magnitude of which is implicitly defined by the constant mass flux condition $\dot{m}_{20} = 0$, where

$$\dot{m}_{20} \equiv |A|^2(\overline{\rho_{20}v_{00}} + \overline{\rho_{00}v_{20}} + 2\overline{\mathrm{Re}\,\{\rho_{11}v_{11}^*\}}), \tag{16}$$

and $\mathrm{Re}\,\{\cdot\}$ denotes the real part of the expression.

4. Results

All numerical results were obtained using 50 spectral modes (see Suslov & Paolucci 1995*b* for a description of the numerical approximation) and the double-precision version of IMSL routine (IMSL 1989) LSBRR.

We consider the spatial mean disturbance distributions given by (14) which can be easily computed in the resonance-free regions (see the discussion of resonances in Suslov & Paolucci 1997*b*). This enables us to augment the disturbance mode analysis based solely on eigenfunctions of the linear problem given in Suslov & Paolucci (1995*b*) by incorporating the lowest-order nonlinear effects. In general, the mean flow distributions change as one proceeds beyond the bifurcation point in the parameter space, but qualitatively they remain the same sufficiently far from the critical point. Thus, it is convenient to analyse the mean flow results for parameters chosen along the linear stability boundaries shown in figure 1. This is done here for the complete range of *Re* considered.

We make clear from the outset that in general when the density of the fluid is allowed to vary, the definition of the Reynolds number (8) based on (9) or (10) results in different values. This difference is presented in figure 2 as a function of the Reynolds number based on (9) (fixed average pressure gradient) and where

$$\dot{m}_{00} = \overline{\rho_{00}v_{00}} \tag{17}$$

is the mass flux associated with the basic flow. We see that the absolute value of this difference increases with the Reynolds number. It can reach up to 5% of the Reynolds number in strongly non-Boussinesq regimes. In general the difference is zero only in the mathematical limit $\epsilon \to 0$ (see figure 2). Thus, in contrast to the Boussinesq limit, and because of our choice of normalization, the basic-flow mass flux

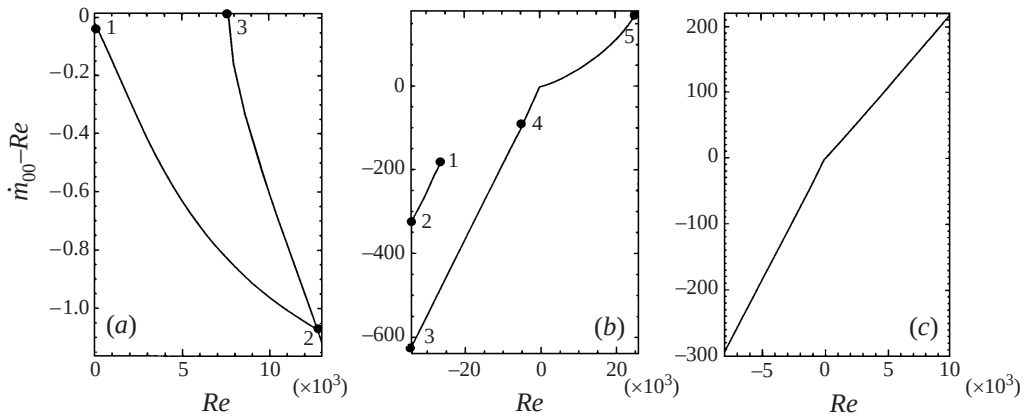

FIGURE 2. Difference between the Reynolds numbers based on fixed average mass flux m_{00} and fixed average longitudinal pressure gradient Re for (a) $\epsilon = 0.005$, (b) $\epsilon = 0.3$ and (c) $\epsilon = 0.6$. Points labelled in (a) and (b) correspond to respective points labelled in figure 1 and are used in the discussion of figures 4–9.

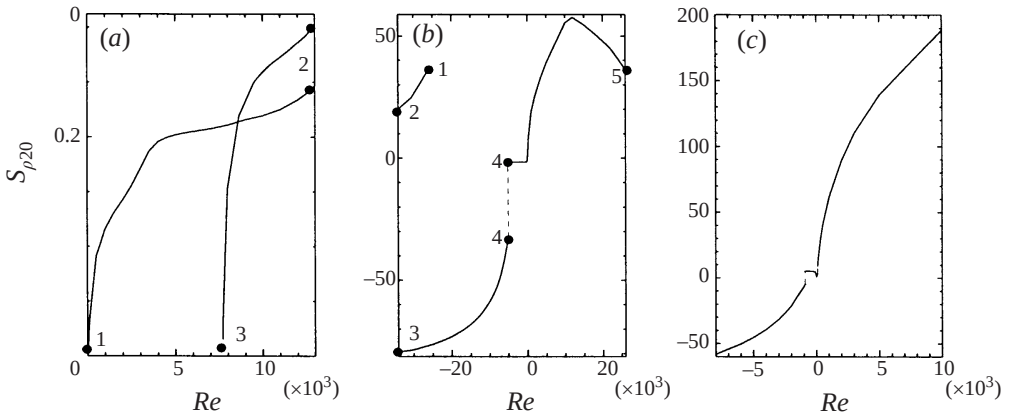

FIGURE 3. Total fluid mass change $S_{\rho 20}$ as a function of the Reynolds number Re estimated along the marginal stability curve shown in figure 1 for (a) $\epsilon = 0.005$, (b) $\epsilon = 0.3$ and (c) $\epsilon = 0.6$. Case of the fixed average longitudinal pressure gradient. Points labelled in (a) and (b) correspond to respective points labelled in figure 1 and are used in the discussion of figures 4–9.

is not an equivalent measure of the Reynolds number; here we have to distinguish between them by introducing definition (17) in addition to that of the Reynolds number. Typically, for non-Boussinesq regimes, and for the chosen equation of state, $|\dot{m}_{00}| \geqslant |Re|$.

Although the quantitative difference in the Reynolds numbers defined for fixed mass flux and longitudinal pressure gradient cases is finite for the non-Boussinesq regimes, our investigation shows that the mean flow results for these two cases are qualitatively similar. Thus, in this work we focus on numerical results obtained for one of these two possible formulations, namely for the case of fixed average pressure gradient unless stated otherwise in the discussion.

4.1. *Total fluid mass variations*

In figure 3, the mass source term $S_{\rho 20}$ is presented as a function of the Reynolds number for several values of ϵ. As follows from (15), the quantity $-S_{\rho 20}$ represents the

change in mass of fluid enclosed within a unit channel length. The numerical value of $|S_{\rho 20}|$ increases substantially in the non-Boussinesq regimes, indicating the stronger dependence of the total mass in the channel upon the magnitude of the developing disturbances for higher values of ϵ. We have found upon evaluating the equilibrium amplitudes and using (15) that when the Grashof number exceeds the critical value by 15% (above supercritical bifurcation points) the actual total fluid mass change in the channel is negligibly small for $\epsilon = 0.005$ and can be up to 0.2% and 1.5% for $\epsilon = 0.3$ and $\epsilon = 0.6$, respectively (see Suslov 1997 for details). Although not shown in the figure, we note that $\lim_{\epsilon \to 0} S_{\rho 20} = 0$, and for small but finite temperature differences between the walls $S_{\rho 20}(Re) \approx -S_{\rho 20}(-Re)$. This symmetry is broken for higher values of ϵ owing to nonlinear density variations and to the appearance of new instability modes. In mixed convection flow ($Re \neq 0$ and $Gr \neq 0$), for all values of ϵ an additional amount of fluid enters and remains within the channel when the average dynamic pressure gradient is positive ($Re < 0$). When the dynamic pressure gradient is reversed ($Re > 0$) in mixed convection flow as well as in the Poiseuille-type flows fluid is discharged from the channel ($S_{\rho 20} > 0$). This is a consequence of the nonlinear density variation with temperature (not shown in the figures) which leads to the larger density disturbance near the hot wall. As a result, when $Re < 0$ the fluid compression near the hot wall, due to the counteracting upward buoyancy force and downward dynamic pressure gradient force, is greater than the fluid expansion near the cold wall, where both buoyancy and pressure forces act downward. When $Re > 0$, the situation is the opposite: the fluid expands near the hot wall more than it compresses near the cold wall, where now the counteraction between the buoyancy and dynamic pressure forces takes place. This shows an indirect relationship between the thermodynamic characteristics of the fluid and the dynamic pressure which, on the surface, seem to be completely decoupled under the low-Mach-number approximation.

4.2. *Mean-flow-correction distributions*

In figures 4–7 we present the mean flow quantities for the disturbed flows. Since the natural convection flow in the vertical channel is very similar to that in the enclosure considered in Suslov & Paolucci (1997*b*), here we focus on the forced and mixed convection cases only. For Poiseuille-type flow, the basic flow and mean flow correction distributions are shown in figure 4. We note that the mean flow correction arising at second order in disturbance amplitude loses symmetry even for very small values of ϵ when fluid properties are allowed to vary. It is also instructive to note from figure 4(*a*) that the cross-channel component of the mean velocity for Poiseuille-type flow is non-zero in contrast to the solution of the conventional Boussinesq equations, where density variation is neglected except in the buoyancy term. As shown in Part 1, the continuity equation for the mean flow correction under non-Boussinesq conditions takes the form

$$\frac{\partial |A|^2}{\partial t_0}(\rho_{20} + S_{\rho 20}) + |A|^2 \mathrm{D}(\rho_{00} u_{20} + 2\mathrm{Re}\{\rho_{11} u_{11}^*\}) = 0. \tag{18}$$

It can be seen from (18) that u_{20} is expected to be zero at steady state only when the density variation ρ_{11} is identically zero as in the Boussinesq equations. As discussed in Suslov & Paolucci (1997*b*), the density disturbance ρ_{11} tends to zero linearly with ϵ and thus so does u_{20}. Indeed, numerical experiments confirm this limiting behaviour. Based on these observations, we may conclude that the range of temperature differences where the standard Boussinesq equations can be used adequately for weakly nonlinear analysis of convection in a realistic fluid might be severely re-

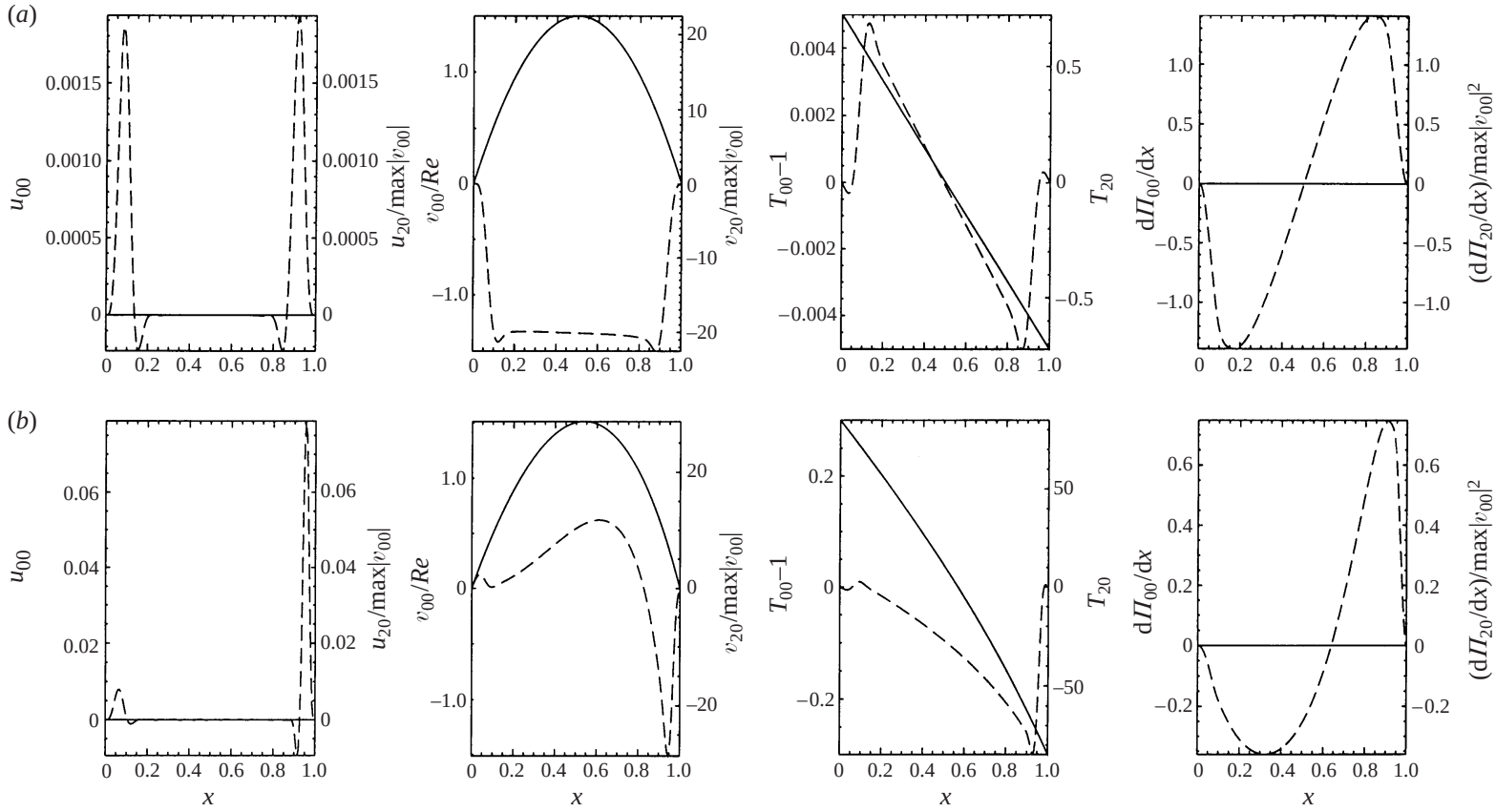

FIGURE 4. Basic-flow (solid lines) and mean-flow-correction (dashed lines) distributions for disturbed Poiseuille-type flows ($Gr = 0$); (*a*) $\epsilon = 0.005$, $Re = 7700$, (*b*) $\epsilon = 0.3$, $Re = 25\,960$.

stricted. Comparing figures 4(*a*) and 4(*b*) we observe a substantial difference between flows in the Boussinesq and non-Boussinesq regimes. Consistent with the discussion in Suslov & Paolucci (1995*b*), in non-Boussinesq regimes the disturbance maximum is located in the region near the cold wall. Two mechanisms are responsible for this asymmetry. For the chosen fluid property variations, both viscosity and thermal conductivity decrease as the local fluid temperature decreases. The lower viscosity leads to a lower diffusion of momentum and thus to higher velocity gradients. The lower thermal conductivity also leads to the appearance of regions of colder and, consequently, denser fluid near $x = 1$ (see the temperature distribution in figure 4*b*). Because of higher thermal conductivity, the mean temperature disturbance near the hot wall is almost zero. Thus, the effect of buoyancy forces near the cold wall favours a stronger downward disturbance flow. Although not shown here, in the Boussinesq limit for negative Reynolds numbers (downward basic flow) the vertical velocity distributions are symmetric with respect to the x-axis in comparison with the ones presented in figure 4. The temperature distributions remain unchanged. In this latter case the buoyancy effects oppose the effects of shear near the cold wall. As a result, non-Boussinesq flow is more stable for negative Reynolds numbers (see figure 1*b*). Note also that in contrast to Boussinesq flow where disturbances always tend to decrease the mean vertical velocity, in non-Boussinesq forced convection (see points 1 and 5 in figure 11*b* and the discussion in § 4.5) the disturbances enhance the vertical flow in the middle part of the channel and thus increase the mass flux through the channel when the average pressure gradient is fixed. The disturbance velocity distributions shown in figure 4 for Poiseuille-type flows reveal almost a singular behaviour near the walls. This indicates that the nonlinear (quadratic) terms arising in the expansions due to the self-interaction of the fundamental disturbance harmonic might become comparable with the magnitude of the linear terms if the amplitude of the disturbance is sufficiently large. In this case the uniformity of expansion (11)–(12) breaks down. This occurs in so-called nonlinear critical layers (see Stuart 1960; Fujimura 1989; Benney & Bergeron 1969; Davis 1969; Benney & Maslow 1974; Haberman 1972) when the disturbance amplitude flows become of order $(\alpha Re)^{-2/3}$ (see Fujimura 1989). In our problem, though, this does not occur for Grashof numbers exceeding the critical one by as much as 15%. In these regimes we estimate $|A_e|(\alpha Re)^{2/3} \lesssim 0.04$ for the complete parameter range considered (Suslov 1997).

As the Grashof and Reynolds numbers increase along line 3–2 in figure 1(*a*), the mean disturbance distributions lose symmetry (see figure 5*a*): while the basic flow velocity maximum moves towards the hot wall since buoyancy enhances the upward motion, the maxima in the disturbance profiles move towards the cold wall where disturbance dissipation processes are weaker owing to lower conductivity and viscosity. At point 2 in figure 1(*a*) another mode, characterized by a smaller wavelength, also becomes unstable according to linear theory. The mean disturbance distributions corresponding to this mode are shown in figure 5(*b*) and are quite similar to the ones just discussed. Consequently, the physical mechanism leading to both types of disturbances is the same and due to the shear associated with the flow, although the shear production mechanisms are different for the two modes. In fact, the shear instability corresponding to line 1–2 in figure 1(*a*) is governed by the buoyancy (flow is destabilized when the Grashof number is increased above line 1–2) while the flow is destabilized because of the larger pressure gradient for the higher Reynolds numbers to the right of line 3–2. The fact that these two modes of instability are very similar to each other from the physical point of view is also confirmed by figure 1(*b*): the

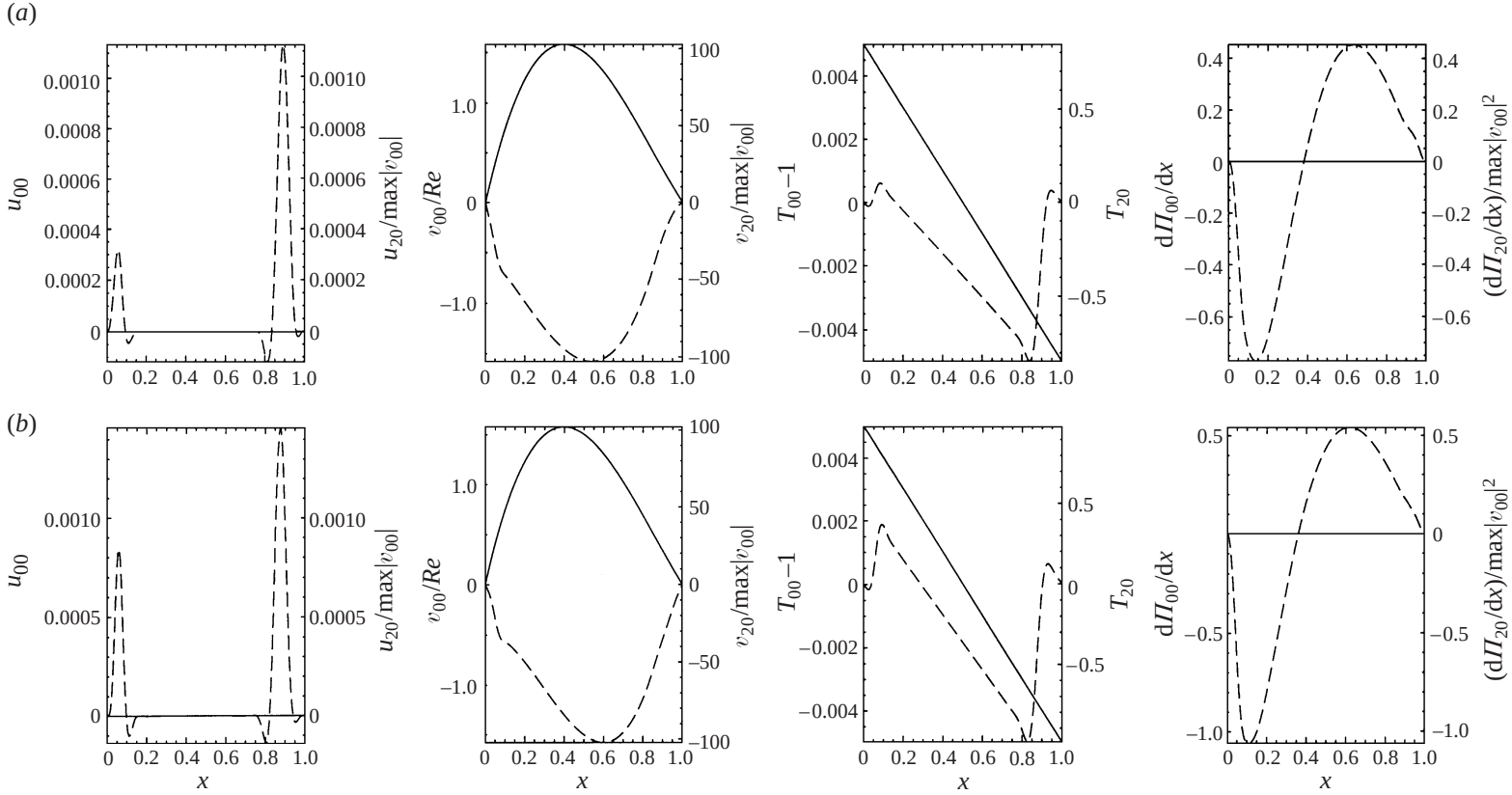

FIGURE 5. Basic-flow (solid lines) and mean-flow-correction (dashed lines) distributions for different instability modes in the vicinity of the codimension-2 point $(Re, Gr) = (12\,850,\ 442\,730)$ at $\epsilon = 0.005$ (point 2 in figure 1*a*); (*a*) $\alpha = 1.6815$, (*b*) $\alpha = 2.1074$.

transition from mixed to purely forced convection becomes smooth in non-Boussinesq regimes (the neighbourhood of point 5).

In the competition between the two instability modes at $\epsilon = 0.3$ (at point 4 in figure 1*b*, also see Suslov & Paolucci 1995*b*) the faster moving (and, consequently, less flow-blocking) mode having a shorter wavelength is preferred for $Re \lesssim -5150$. The mean flow distributions corresponding to the different instabilities are shown in figure 6. Since the physical mechanism for both instabilities is the same, the qualitative behaviour of the mean flow correction quantities is similar for both modes, although the shorter-wavelength mode has a much more evident roll structure than the longer-wavelength mode. In fact, as can be seen from the first two columns of figure 6, the relative role of transverse motion is stronger for the shorter-wavelength mode. Thus, as the absolute value of Reynolds and Grashof numbers increases along line 0–4–3 in figure 1(*b*), the rolls, which arise from the shear instability, are stretched to such an extent that the velocity disturbances are essentially longitudinal. This is discussed in more detail in Suslov & Paolucci (1995*b*) and shown there in figure 12. At point 4 each of these long rolls breaks into smaller rolls with a wavelength approximately fifteen times shorter and moving with a larger wave speed downstream.

In the strongly non-Boussinesq regime corresponding to $\epsilon = 0.6$, a competition between the shear- and buoyancy-driven instability modes occurs. As discussed in Suslov & Paolucci (1995*b*), the buoyant instability is characterized by a much longer wavelength than the shear instability and arises due to the nonlinear density variation with temperature. When the flow becomes unstable due to the buoyant disturbance, a colder fluid region exists near the middle of the channel. This can be seen from the temperature distribution shown in figure 7(*a*). The buoyancy force acting on this colder and denser core causes a strong downward disturbance flow (see the second plot in figure 7*a*). The associated transverse motion is much weaker than that of the shear-driven instability (compare plots in the two left-hand columns in figure 7). The wave speed of the buoyancy-driven disturbance is always negative (Suslov & Paolucci 1995*b*). When the absolute value of the Reynolds number is increased ($Re \lesssim -860$ or $Re \gtrsim 88$) the shear instability begins to dominate so that the rolls move in the direction of the primary flow as shown in Suslov & Paolucci (1995*b*).

4.3. *Average kinetic energy*

In figure 8 we present the average kinetic energy of the flow. As in Suslov & Paolucci (1997*b*), we define

$$\langle E_k \rangle = \langle E_{k00} \rangle + |A|^2 \langle E_{k20} \rangle + O\left(|A|^4\right), \tag{19}$$

where

$$\langle E_{k00} \rangle = \tfrac{1}{2}\overline{\rho_{00} v_{00}^2}, \tag{20}$$

$$\langle E_{k20} \rangle = [\overline{\rho_{00}\left(|u_{11}|^2 + |v_{11}|^2 + v_{00}v_{20}\right)} + 2\overline{v_{00}\,\mathrm{Re}\left\{\rho_{11} v_{11}^*\right\}} + \tfrac{1}{2}\overline{\rho_{20} v_{00}^2}]. \tag{21}$$

The basic-flow kinetic energy scale is chosen in such a way that its value is of the same order for the two limiting cases of natural and forced convection. For all values of ϵ we observe that the instability first occurs for a substantially less energetic flow when the basic flow field is generated primarily by buoyancy forces (essentially natural convection). The shear disturbances in the majority of cases decrease the total kinetic energy of the flow (the ratio $\langle E_{k20} \rangle / \langle E_{k00} \rangle$ is negative), although the kinetic energy of the non-Boussinesq Poiseuille-type flows is slightly increased since, as will be shown in figure 11 and discussed in § 4.5, the total mass flux through the channel increases in these regimes owing to the developing disturbances. The buoyant

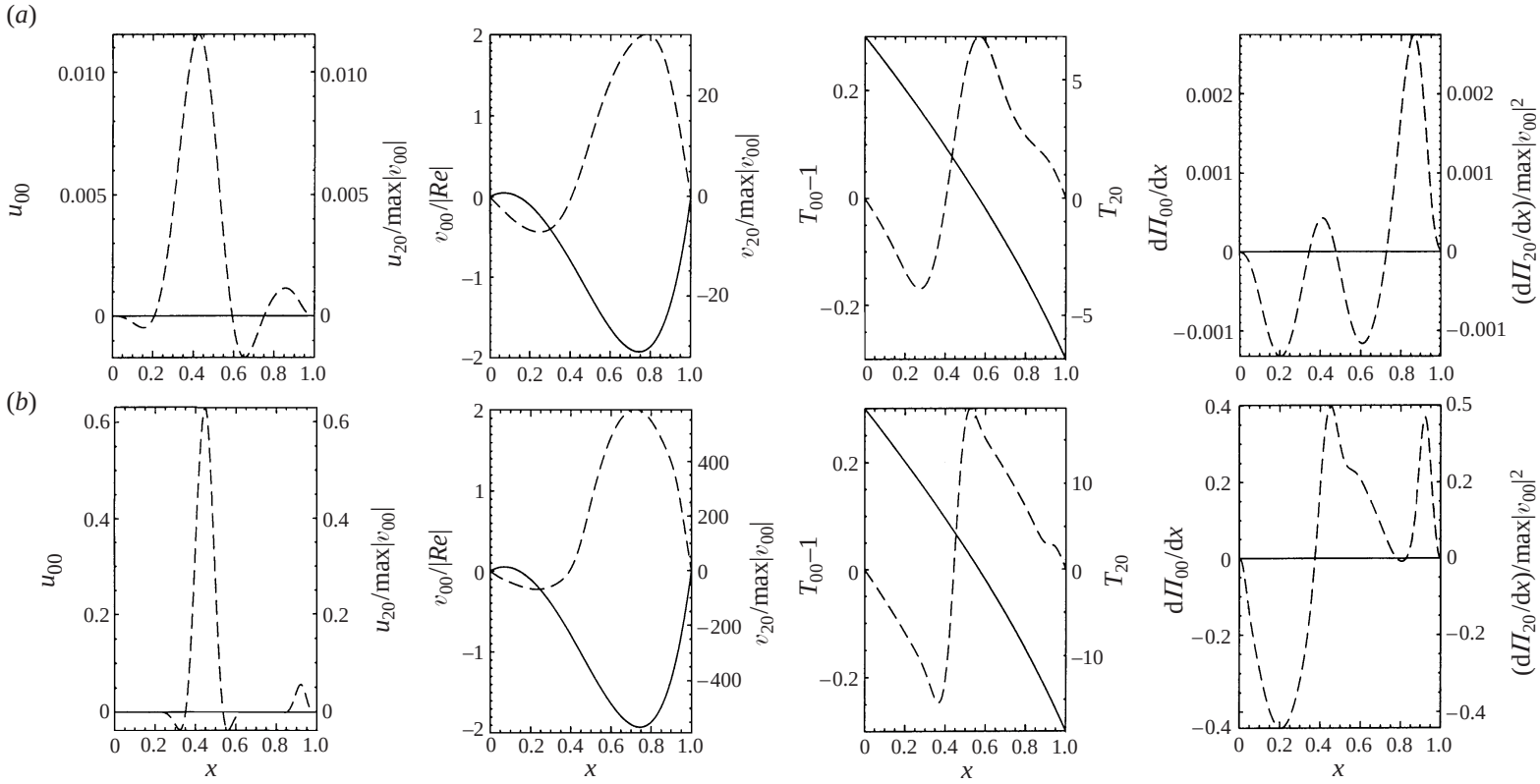

FIGURE 6. Basic-flow (solid lines) and mean-flow-correction (dashed lines) distributions for different instability modes in the vicinity of the codimension-2 point $(Re, Gr) = (-5150,\ 524\,640)$ at $\epsilon = 0.3$ (point 4 in figure 1*b*); (*a*) $\alpha = 0.0800$, (*b*) $\alpha = 1.1828$.

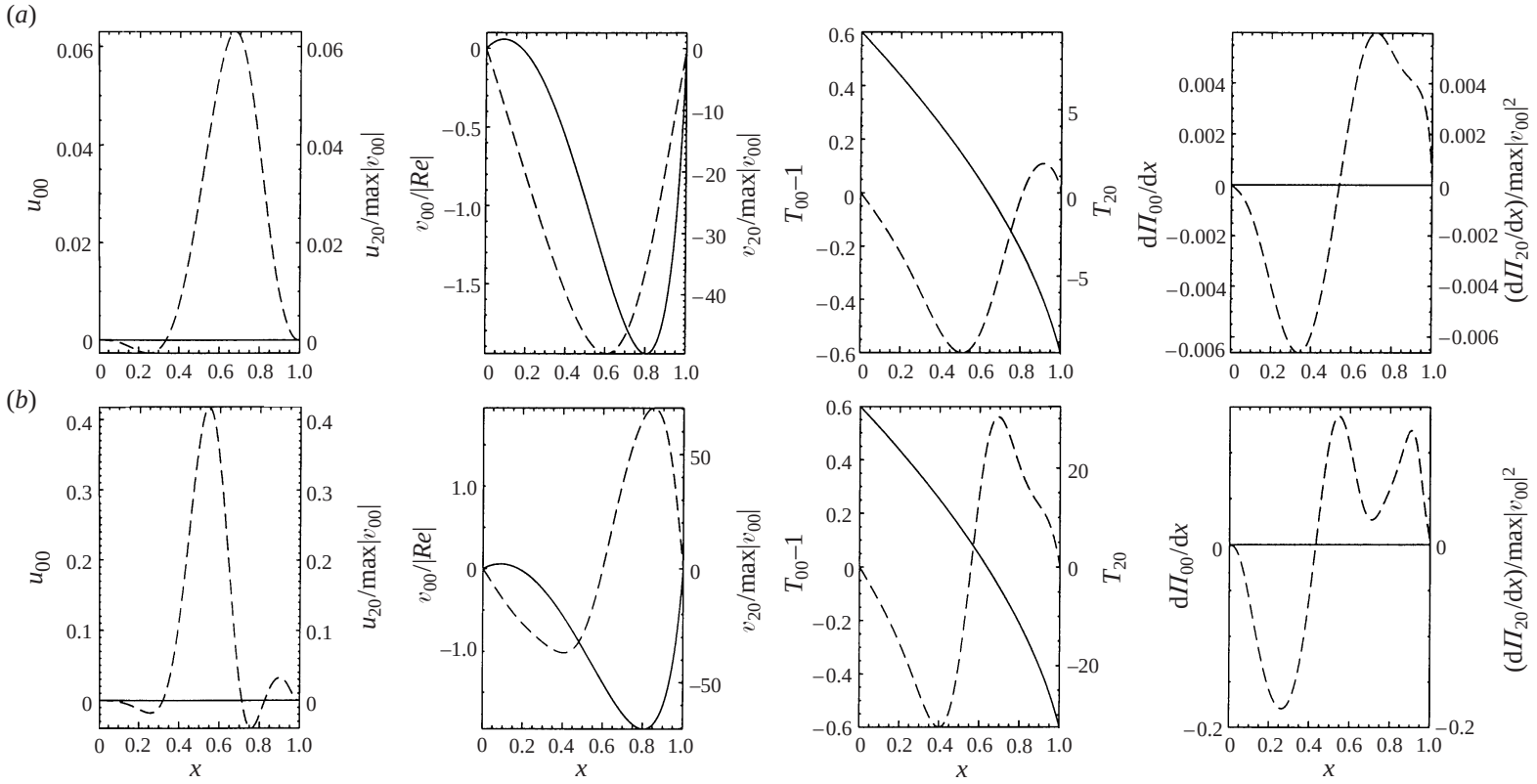

FIGURE 7. Basic-flow (solid lines) and mean-flow-correction (dashed lines) distributions for different instability modes in the vicinity of the codimension-2 point $(Re, Gr) = (-860, 95\,032)$ at $\epsilon = 0.6$; (*a*) buoyant instability, $\alpha = 0.1000$, (*b*) shear instability, $\alpha = 0.6285$.

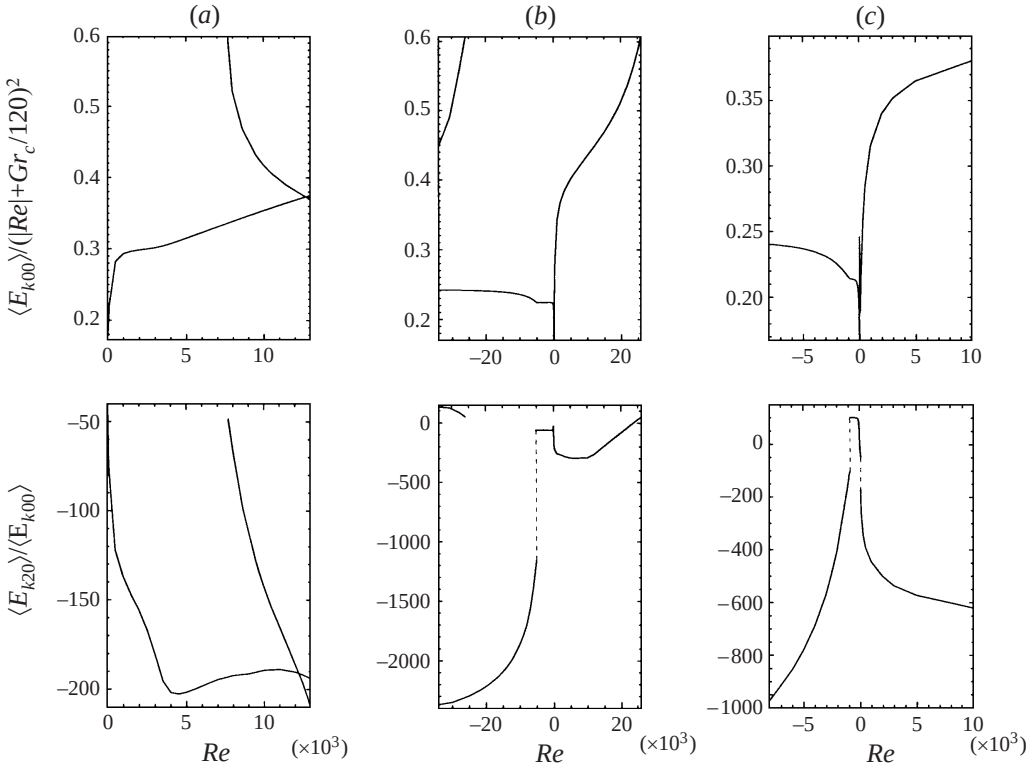

FIGURE 8. Basic-flow (upper row) and mean-flow-correction (lower row) kinetic energy at critical points (see figure 1) as functions of Reynolds number for (*a*) $\epsilon = 0.005$, (*b*) $\epsilon = 0.3$ and (*c*) $\epsilon = 0.6$.

disturbance appearing in highly non-Boussinesq regimes, as in the case of convection in a closed cavity (Suslov & Paolucci 1997*b*), leads to more energetic motion in the direction of gravity thus increasing the average flow kinetic energy for negative Reynolds numbers. For positive Reynolds numbers, the pressure and buoyancy forces oppose each other and as a consequence this competition gives rise to a less energetic flow. Note that when the average pressure gradient is fixed, it is the mass flux through the channel which defines largely the disturbance kinetic energy: the distributions of relative average disturbance kinetic energy $\langle E_{k20}\rangle/\langle E_{k00}\rangle$ are qualitatively very similar to the relative average mass flux curves presented in figure 11.

Estimation of equilibrium amplitudes for a Grashof number 15% larger than the critical value (Suslov & Paolucci 1995*b*) with (19) enables us to conclude that the average kinetic energy of the forced convection flow changes just slightly (less than 1%) from the basic flow values for all regimes. The change is much greater for natural convection. In that case shear disturbances decrease the average flow kinetic energy by about 10% for $\epsilon = 0.005$ and $\epsilon = 0.3$, while buoyant disturbances increase the flow kinetic energy by more than 30% for $\epsilon = 0.6$.

To complete our discussion of the average energy of the disturbed flow, we note that the thermal energy of the flow, which is defined by the thermodynamic pressure (see Suslov & Paolucci 1997*b*), remains constant as the disturbances develop, since under low-Mach-number conditions the thermodynamic pressure in an open system remains constant if the ambient pressure is not changing.

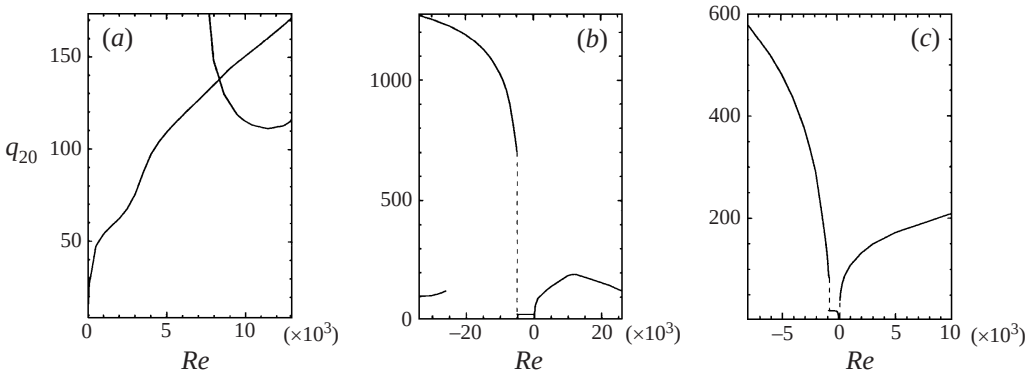

FIGURE 9. Mean-flow-correction heat flux at critical points (see figure 1) as a function of Reynolds number for (*a*) $\epsilon = 0.005$, (*b*) $\epsilon = 0.3$ and (*c*) $\epsilon = 0.6$.

4.4. *Average heat flux across the channel*

In this subsection we look at the average heat flux across the channel. The conduction heat flux, defined as

$$q_c = q_{00} = -\frac{1}{2\epsilon} k_{00}\, \mathrm{D}T_{00}\bigg|_{x=1} \tag{22}$$

is computed in Suslov & Paolucci (1997*b*) for values of $0 < \epsilon \leqslant 0.6$. It is shown there that the conduction heat flux depends slightly on the value of the temperature difference between the walls and remains very close to unity (see figure 11 in Suslov & Paolucci 1997*b*). The mean-flow-correction heat flux is given by

$$q_{20} = -\frac{1}{2\epsilon} k_{00}\, \mathrm{D}T_{20}\bigg|_{x=1}. \tag{23}$$

Consequently, the average Nusselt number which represents the average cross-channel heat flux for a periodically disturbed flow can be computed from

$$Nu = Nu(Gr, Re, \epsilon) = \frac{1}{q_c}\left[\ \frac{1}{\lambda}\int_{y_0-\lambda/2}^{y_0+\lambda/2} q\, \mathrm{d}y\ \right]_{x=1} \approx 1 + |A_e|^2 \frac{q_{20}}{q_{00}} \tag{24}$$

for any set of parameters. Our estimations show that for Grashof numbers 15% larger than the critical value the Nusselt number increase due to the developing shear disturbances in the case of large longitudinal pressure gradients can be up to 40%. In contrast, in the natural convection case the Nusselt number increment is about 3% for $\epsilon = 0.005$ and it grows to about 5% for $\epsilon = 0.6$. More detailed numerical results for the average Nusselt number will be given later in this section.

The deviation from the conductive heat flux in the vicinity of the bifurcation points is presented in figure 9 for different values of ϵ and for Gr_c along the curves shown in figure 1 as a function of the Reynolds number. Its value is always positive and, as expected, bifurcation associated with any disturbance mechanism leads to enhanced heat transfer across the channel. Note also that a much more rapid heat flux increase is expected after instability occurs for negative Reynolds numbers than for positive ones in non-Boussinesq regimes. Another point to note from figure 9(*c*) is that the buoyancy instability mode affects the heat flux to a much lower degree than the shear-driven instability mode since the mean-flow-correction temperature gradient associated with it is lower (see figure 6).

Re	β_{Gr}			$\lvert\beta_{Re}\rvert$		
	Present results		Fukui *et al.*	Present results		Fukui *et al.*
	$\hat{\Pi}^* = \text{const.}$	$\dot{m}^* = \text{const.}$	$\dot{m}^* = \text{const.}$	$\hat{\Pi}^* = \text{const.}$	$\dot{m}^* = \text{const.}$	$\dot{m}^* = \text{const.}$
0	0.324	0.324	0.6508	0.000	0.000	—
20	0.329	0.324	0.6568	0.010	0.010	0.0008
40	0.344	0.325	0.6724	0.040	0.037	0.0050
60	0.369	0.327	0.6940	0.086	0.076	0.0154
80	0.395	0.328	0.7168	0.139	0.116	0.0317
100	0.404	0.327	0.7380	0.186	0.149	0.0515

TABLE 1. Comparison of the present results for the slopes of the Nusselt number curves evaluated at the critical points $Gr_c(Re)$ for $\epsilon = 0.005$ with computations of Fukui *et al.* (1982) in the Boussinesq limit ($\hat{\Pi}^* = \text{const.}$ and $\dot{m}^* = \text{const.}$ correspond to the cases of fixed average longitudinal pressure gradient and fixed average mass flux respectively).

Since for fixed ϵ both $|A_e|$ and q_{20} entering (24) depend on Gr and Re, so does Nu. Thus, in order to provide the quantitative results for a range of parameters close to the critical ones we follow Fukui *et al.* (1982) and introduce the coefficients

$$\beta_{Gr}(Re,\epsilon) = \left.\frac{\partial Nu}{\partial \delta_{Gr}}\right|_{(Gr_c(Re,\epsilon)\,Re,\,\epsilon)}, \quad \beta_{Re}(Re,\epsilon) = \left.\frac{\partial Nu}{\partial \delta_{Re}}\right|_{(Gr_c(Re,\epsilon),\,Re,\,\epsilon)} \tag{25}$$

evaluated at the critical points. These coefficients enable one to estimate linearly the actual value of Nu at the point (Gr, Re', ϵ) in the vicinity of the critical point $(Gr_c(Re,\epsilon), Re, \epsilon)$ as

$$Nu(Gr, Re', \varepsilon) \approx 1 + \beta_{Gr}\delta_{Gr} + \beta_{Re}\delta_{Re}, \tag{26}$$

where

$$\delta_{Gr} = Gr/Gr_c(Re,\epsilon) - 1, \quad \delta_{Re} = Re'/Re - 1. \tag{27}$$

The numerical values of (25) are obtained using two-point finite difference approximations of partial derivatives of (24) with $\delta_{Gr,Re} = 10^{-4}$. In the Boussinesq limit $\epsilon \to 0$ and for $Re = 0$, owing to the symmetry of the basic flow velocity profile the flow considered in the present work becomes identical to that in a tall closed cavity. This is confirmed by the agreement between the value of $\beta_{Gr} = 0.324$ given in table 1 and the value of 0.34 reported in Suslov & Paolucci (1997*b*) on the flow in an enclosure (the slight discrepancy is due to the fact that a larger number of spectral modes is used in the present investigation). Comparison of the present results with those reported by Fukui *et al.* (1982) for $Pr = 0.7$ and Boussinesq mixed convection flow in a differentially heated vertical channel is given in table 1. While in qualitative agreement, our results differ quantitatively from those by Fukui *et al.* (a similar discrepancy was noted in Suslov & Paolucci (1997*b*). The possible reason for this discrepancy is that Fukui *et al.* assume that the flow preserves its spatial structure predicted by linear analysis for infinitesimal disturbances even in the case when the amplitude is finite, while in our approach we also take into account the contribution of the second harmonic which is due to the nonlinear self-interaction of the fundamental disturbance wave.

It is instructive to compare our predictions with experimental results. For Boussinesq convection flow of air in a tall vertical differentially heated cavity, ElSherbiny, Raithby & Hollands (1982) provide the following empirical correlation formula for

the Nusselt number:

$$Nu = \left[1 + (0.0607 Ra^{1/3})^{18}\right]^{1/18} \quad \text{for} \quad L/H = 110, \quad Ra < 1.2 \times 10^4, \tag{28}$$

where $Ra = GrPr$ is the Rayleigh number. Other correlations are available in the literature, but they are given for a wider range of the Rayleigh number (see Shewen, Hollands & Raithby 1996, for example) and as a result are less accurate in the vicinity of the bifurcation point. In order to compare our predictions with the experimental data we first define the experimental 'bifurcation' point $Ra_c^{exp.}$. It is necessary since the transition from the conduction to the convection state in experimental conditions is not abrupt (imperfect bifurcation) in contrast to what is predicted by linear stability analysis. We estimate the value of $Ra_c^{exp.}$ to correspond to the inflection point in the correlation. At this location, the slope of the Nusselt number curve is maximum, which is also the case when the theoretical pitchfork bifurcation is considered and the slope is computed at the critical point (the theoretical value for the critical Rayleigh number Ra_c in the Boussinesq limit is 5706.7). Then

$$\delta_{Gr}^{exp.} = Ra_c^{exp.} \left.\frac{\mathrm{d}Nu}{\mathrm{d}Ra}\right|_{Ra = Ra_c^{exp.}}, \quad \text{where} \quad \left.\frac{\mathrm{d}^2 Nu}{\mathrm{d}Ra^2}\right|_{Ra = Ra_c^{exp.}} = 0. \tag{29}$$

Using the above correlation formula we obtain $\delta_{Gr}^{exp.} = 0.331$ for $Ra_c^{exp.} = 6256$. The relative discrepancy between the value estimated from the correlation formula and the theoretical critical Rayleigh number is 10%. The discrepancy between our value of 0.324 and the correlation Nusselt number coefficient is 2% while the result of Fukui *et al.* differs by 97% from the experiment. Thus our prediction is in much better agreement with the experimental data in Boussinesq natural convection, but a more accurate experiment in the vicinity of the transition is necessary to better estimate the actual accuracy of our prediction. Unfortunately, to the authors' knowledge such accurate experimental data are not available at the moment.

We also note from table 1 that according to our computations the Nusselt number coefficient in the case of fixed mass flux changes less as the Reynolds number increases than in the case of fixed pressure gradient. This is because in the former situation, as was discussed earlier, disturbances are more restricted in their growth and their equilibrium amplitudes are smaller.

In figure 10 we show the Nusselt number coefficients estimated at the critical points as functions of Reynolds number over a much wider range. Results are given only for regions where the bifurcation from parallel to wavy periodic flow is supercritical ($K_1^R < 0$, see Part 1). Note that, as follows from (27), negative values of β_{Gr} or β_{Re} correspond to cases when a parallel flow bifurcates to a periodic one as $|Gr|$ or $|Re|$, respectively, is decreased. The Nusselt number coefficients increase rapidly in the vicinity of points where a change from supercritical to subcritical bifurcations occurs. In these regions higher-order terms in the expansions have to be retained for adequate predictions of the equilibrium disturbance amplitude. Since this is not done in the current paper the $\beta_{Gr,Re}$-curves in figure 10 are truncated. The two branches in figure 10(*a*) correspond to thermally driven (left) and pressure-driven Poiseuille-type (right) flows in the Boussinesq limit (note that because of the symmetry with respect to the Reynolds number, results are presented only for positive values of Re). Here, flows characterized by large values of Gr and relatively small Re are called thermally driven, while those with Re larger than the critical value for a pure Poiseuille flow ($Re_c \approx 7696.3$ in our non-dimensionalization) and small Gr are called Poiseuille-type flows. Consistent with the discussion in Fukui *et al.* (1982), for thermally driven flow

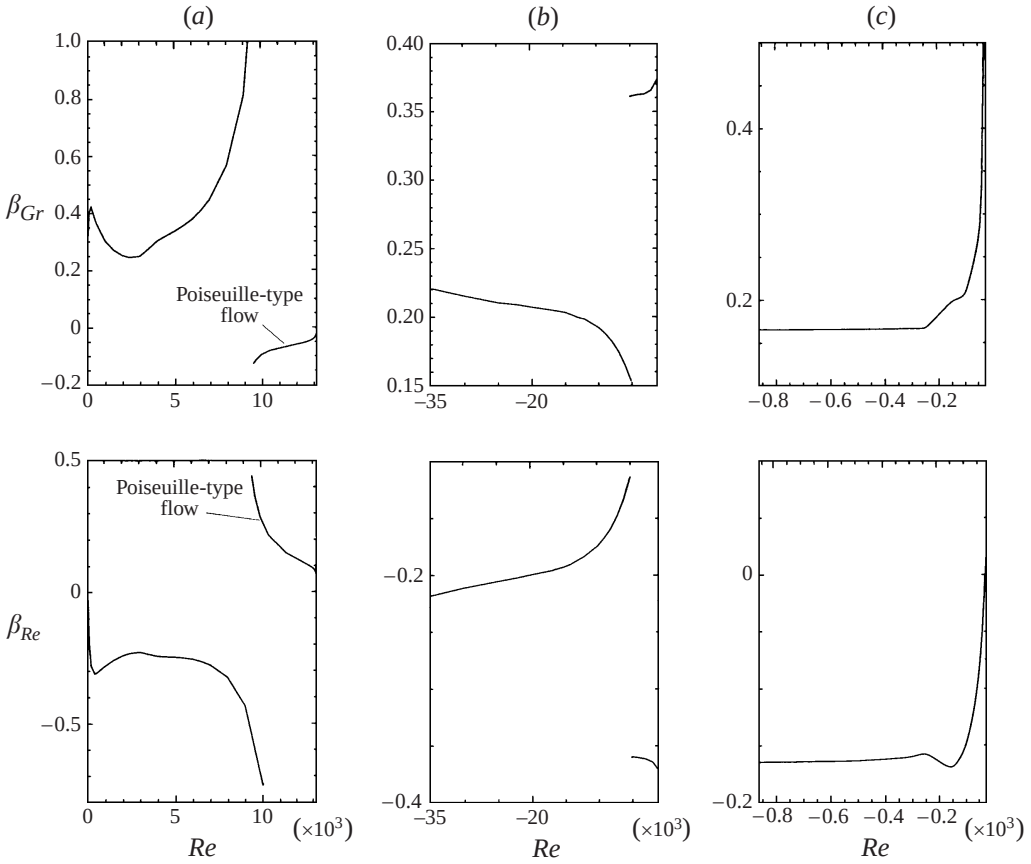

FIGURE 10. Nusselt number coefficients for regions of supercritical bifurcations as functions of Reynolds number for (*a*) $\epsilon = 0.005$, (*b*) $\epsilon = 0.3$ and (*c*) $\epsilon = 0.6$.

the Grashof number influence on the channel heat transfer rate is stronger than that of the Reynolds number ($|\beta_{Gr}| > |\beta_{Re}|$). The situation is opposite for the Poiseuille-type flows. This emphasizes the different physical nature of the heat flux enhancement mechanisms found in the different regions of parameter space.

The two branches in figure 10(*b*) represent two different shear instabilities occurring in the downward mixed convection flow in the slightly non-Boussinesq regime. The curves are truncated in the vicinity of the codimension-2 point where a two-mode interaction analysis is necessary to provide proper numerical predictions. This is again beyond the scope of the present work. As seen from figure 10(*b*) effects of *Gr* and *Re* on the heat flux become equally important ($|\beta_{Gr}| \sim |\beta_{Re}|$) when the temperature difference between the walls is increased. Additionally we see that the long-wave shear instability, which is dominant for smaller $|Re|$ (Suslov & Paolucci 1995*b*), intensifies the heat transfer between the walls to a larger degree than the short-wave shear instability which dominates at higher $|Re|$ (Suslov & Paolucci 1995*b*). This result is anticipated since, as noted in Part 1, long-wave disturbances have larger amplitudes. The heat transfer associated with the short-wave instability increases as the shear in the basic flow becomes larger with increase in $|Re|$.

In the strongly non-Boussinesq regime, bifurcations associated with the shear instability are always subcritical. Thus in figure 10(*c*) we present the Nusselt number

coefficients only for the buoyant instability. In contrast to the shear modes, the buoyant instability effect on the average Nusselt number depends weakly on the Reynolds number except in the nearly natural convection regime ($|Re| \approx 0$). There the effect of the imposed pressure gradient on the heat flux becomes negligible ($|\beta_{Re}| \to 0$) while the sensitivity of the Nusselt number to changes in Grashof number increases substantially. The sharp increase in β_{Gr} for small $|Re|$ is also partly due to the closeness of the point where the bifurcation type changes from supercritical to subcritical.

4.5. *Average mass flux through the channel*

The average fluid mass flux through the channel is another characteristic of the flow of practical importance when the average longitudinal pressure gradient is maintained fixed. Figure 11 shows the ratio of the mean mass flux correction to the basic-flow mass flux which enters the expression for the total average mass flux

$$\dot{m} = \dot{m}_{00}\left[1 + \frac{\dot{m}_{20}}{\dot{m}_{00}} + O(|A|^4)\right] \tag{30}$$

(here $\dot{m}_{20}$ is computed using (16) with $|A| = 1$ and $\dot{m}_{00}$ is defined by (17)). This ratio is singular near $Re = 0$, where $\dot{m}_{00} = 0$ and $\dot{m}_{20} \neq 0$ (obviously, this singularity is removable in (30)), and is always negative for Boussinesq convection, meaning that the developing disturbance rolls (which are primarily caused by shear instability of the basic flow, see Suslov & Paolucci 1995*b*) tend to block the channel, thus decreasing the total mass flux when the pressure difference between the channel inlet and outlet is kept fixed. For the most part, this remains the case for the range of parameter space explored in non-Boussinesq flows. The only exception is in the narrow region near $Re = 0$ and for flows of Poiseuille type ($Gr \approx 0$), where developing disturbances enhance the total mass flux. For small Reynolds numbers this is a direct consequence of the nonlinear correlation between the disturbance density variation across the channel and the velocity field: while the disturbance velocity tends to reduce the total shear of the flow (i.e. the velocity gradient) and, consequently, the maximum flow velocity (see figures 4–6 in Suslov & Paolucci 1997*b*), the thermal disturbances lead to an increase in local density of the fluid such that the net effect on the mass flux is positive. Poiseuille-type flows will be considered in more detail later.

The actual change in mass flux can be computed using (30) after the disturbance amplitude is found. Our investigation shows that, for instance, when the Grashof number exceeds the critical value by 15% (in supercritical bifurcations) the maximum average mass flux change due to developing disturbances is about 1%, 4% or 15% compared with the undisturbed flow for $\epsilon = 0.005$, $\epsilon = 0.3$ and $\epsilon = 0.6$, respectively, (see Suslov 1997 for details).

Similarly to the previous section, we approximate the average mass flux linearly in the vicinity of bifurcation points as

$$\dot{m}(Gr', Re', \epsilon) \approx \dot{m}_{00}(Gr_c(Re, \epsilon), Re, \epsilon)(1 + \gamma_{Gr}\delta_{Gr} + \gamma_{Re}\delta_{Re}), \tag{31}$$

where the mass flux coefficients

$$\left.\begin{aligned} \gamma_{Gr}(Re, \epsilon) &= \frac{\partial}{\partial \delta_{Gr}}\left(\frac{\dot{m}_{20}}{\dot{m}_{00}}\right)\Bigg|_{(Gr_c(Re,\epsilon),\, Re,\, \epsilon)}, \\ \gamma_{Re}(Re, \epsilon) &= \frac{\partial}{\partial \delta_{Re}}\left(\frac{\dot{m}_{20}}{\dot{m}_{00}}\right)\Bigg|_{(Gr_c(Re,\epsilon),\, Re,\, \epsilon)} \end{aligned}\right\} \tag{32}$$

are evaluated at the critical points.

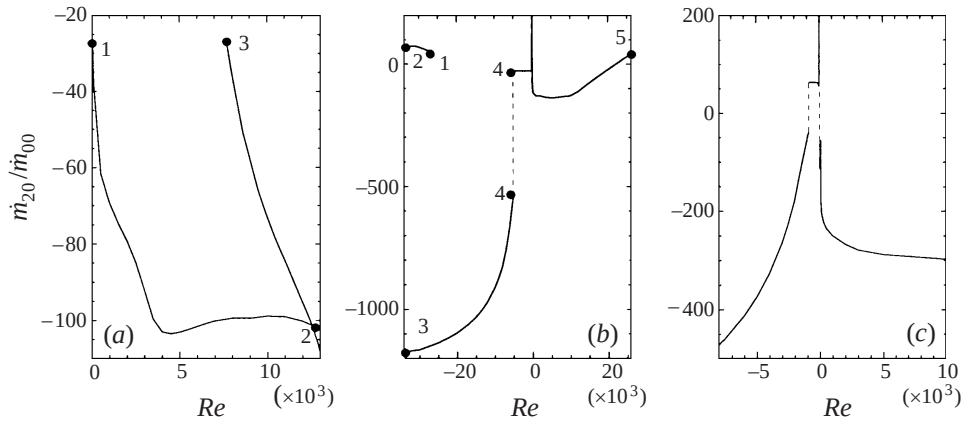

FIGURE 11. Relative mean flow variation for the fixed average pressure gradient case at critical points as a function of Reynolds number for (*a*) $\epsilon = 0.005$, (*b*) $\epsilon = 0.3$, and (*c*) $\epsilon = 0.6$. Points labelled in (*a*) and (*b*) correspond to respective points labelled in figure 1 and are used in the discussion of figures 4–9.

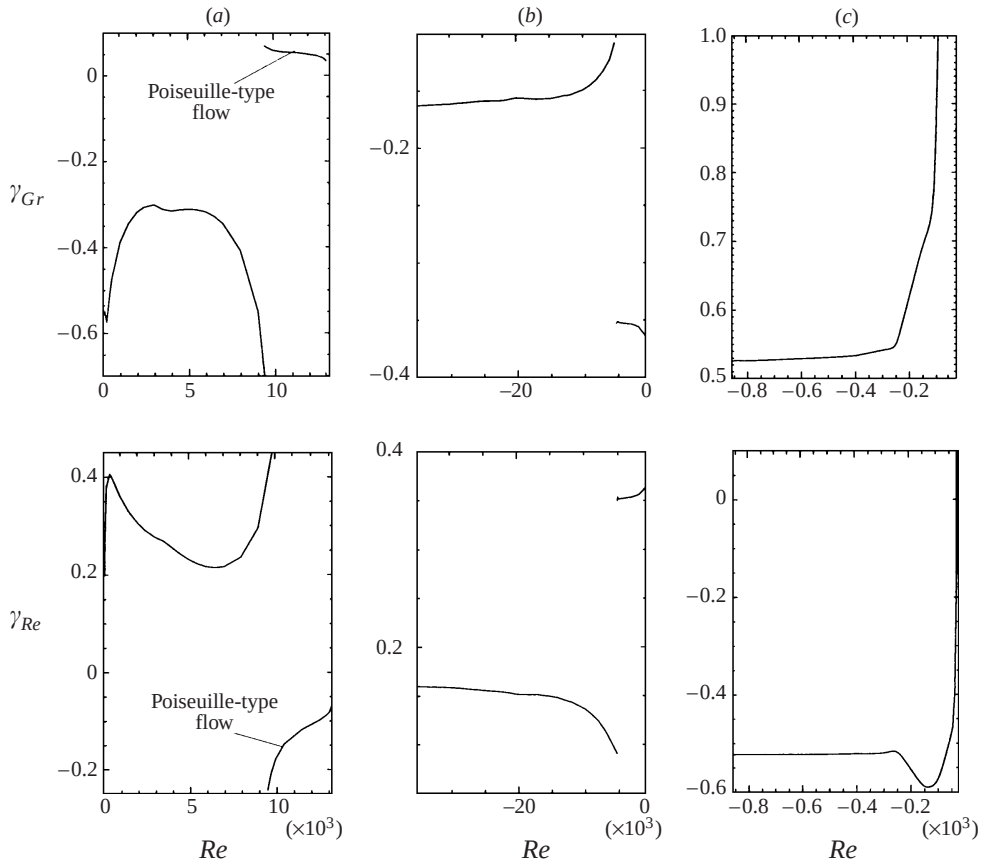

FIGURE 12. Average mass flux coefficients for regions of supercritical bifurcations as functions of Reynolds number for (*a*) $\epsilon = 0.005$, (*b*) $\epsilon = 0.3$, and (*c*) $\epsilon = 0.6$.

In figure 12 we show the average mass flux coefficients estimated at the critical points as functions of Reynolds number. Results are given for the same parameter ranges as for the Nusselt number. As in figure 10(*a*), the two branches in figure 12(*a*) correspond to thermally driven (left) and pressure-driven Poiseuille-type (right) flows in the Boussinesq limit. Note that $\delta_{Gr} > 0$ and $\delta_{Re} < 0$ for thermally driven flows, while $\delta_{Gr} < 0$ and $\delta_{Re} > 0$ for Poiseuille-type flows. Thus the products $\gamma_{Gr}\delta_{Gr}$ and $\gamma_{Re}\delta_{Re}$ are always negative. We conclude that, in the Boussinesq limit, for the complete range of Reynolds numbers, developing disturbances decrease the mass flux through the channel. Indeed rolls produced by instability induce cross-channel motion and result in a blocking effect to the longitudinal flow.

For both instability branches in the weakly non-Boussinesq regime depicted in figure 12(*b*), $\delta_{Gr} > 0$ and $\delta_{Re} < 0$. Thus, similar to Boussinesq mixed convection flows, instabilities arising when the temperature difference between the walls is moderate lead to a similar flow-blocking effect. As discussed in Suslov & Paolucci (1995*b*), both instabilities arising in the downward mixed convection flow at moderate temperature differences between the walls have the same physical nature – shear. Earlier in this paper we suggested that the major selection mechanism between these two instabilities is the tendency of the flow to adjust to a state with smaller flow-blocking effect as the intensity of the primary flow increases. Figure 12(*b*) confirms this conclusion: as the absolute value of the Reynolds number increases, the dominant instability pattern changes in such a way that the mean mass flux is affected by the developing instability rolls to a much smaller degree (both mass flux coefficients decrease by a factor of about 3.5 at the codimension-2 point).

Finally, in figure 12(*c*) we present the average mass flux coefficients for the buoyant instability arising at small negative Reynolds numbers. The nearly singular behaviour of the coefficients for Reynolds numbers close to zero is due to our normalization combined with the fact that the basic-flow mean mass flux $\dot{m}_{00}$ tends to zero (see definitions (32) and earlier discussion). Since in this regime $\delta_{Gr} > 0$ and $\delta_{Re} < 0$ we conclude that the buoyancy effects associated with a strong nonlinear density variation in non-Boussinesq regimes enhance the mean flow in the direction of gravity.

5. Summary

A weakly nonlinear theory which we have developed in Part 1 for the analysis of low-Mach-number flows in open domains has been applied to predict average characteristics of the flow of air in an open vertical channel with differentially heated walls for a wide range of governing parameters in non-Boussinesq natural, forced and mixed convection. The detailed linear stability results for distinct shear- and buoyancy-driven instabilities given in Suslov & Paolucci (1995*b*) are complemented with corresponding mean flow energetics in past bifurcation states. Based on the values of the equilibrium disturbance amplitudes estimated in the regions of supercritical bifurcations using the cubic Landau equation we provide numerical data for the average mass flux through the channel and for the average Nusselt number for the heat flux across the channel. These data are shown to be in encouraging agreement with experimental results available for Boussinesq convection. The authors hope that the very rich behaviour of non-Boussinesq convection flow discovered analytically will inspire experimental research in this area, which to the authors' knowledge has not been undertaken to date. Experiments on accurate determination of quantitative characteristics of the disturbed flow such as the average Nusselt number in the vicinity of the bifurcation point would be especially valuable to estimate the accuracy

of the present theory. Experiments for large temperature differences between the walls similar to the ones conducted by Fukui *et al.* (1982) are necessary to investigate the influence of fluid property variations on the flow pattern, especially in regimes where the theory predicts the existence of codimension-2 points with competing instabilities of different physical nature.

REFERENCES

Benney, D. J. & Bergeron, R. F. 1969 A new class of nonlinear waves in parallel flows. *Stud. Appl. Maths* **48**, 181–204.

Benney, D. J. & Maslow, S. A. 1974 The evolution in space and time of nonlinear waves in parallel shear flows. *Stud. Appl. Maths* **54**, 181–205.

Davis, R. E. 1969 On the high Reynolds number flow over a wavy boundary. *J. Fluid Mech.* **36**, 337–346.

ElSherbiny, S., Raithby, G. & Hollands, K. 1982 Heat transfer by natural convection across vertical and inclined air layers. *Trans. ASME* : *J. Heat Transfer* **104**, 96–102.

Fujimura, K. 1989 The equivalence between two perturbation methods in weakly nonlinear stability theory for parallel shear flows. *Proc. R. Soc. Lond.* A **424**, 373–392.

Fukui, K., Nakajima, M., Ueda, H., Suzaki, K. & Mizushina, T. 1982 Flow instability and transport phenomena in combined free and forced convection between vertical parallel plates. *J. Chem. Engng Japan* **15**, 172–180.

Haberman, R. 1972 Critical layers in parallel flows. *Stud. Appl. Maths* **51**, 139–161.

Herbert, T. 1983 On perturbation methods in nonlinear stability theory. *J. Fluid Mech.* **126**, 167–186.

IMSL, Inc. 1989 *IMSL Mathematical Library, Version 1.1*. Houston, TX.

Paolucci, S. 1982 On the filtering of sound from the Navier–Stokes equations. *Tech. Rep.* SAND82-8257. Sandia National Laboratories, Livermore, California.

Shewen, E., Hollands, K. & Raithby, G. 1996 Heat transfer by natural convection across a vertical air cavity of large aspect ratio. *Trans. ASME* : *J. Heat Transfer* **118**, 993–995.

Stuart, J. T. 1960 On the non-linear mechanics of wave disturbances in stable and unstable parallel flows. Part 1. The basic behaviour in plane Poiseuille flow. *J. Fluid Mech.* **9**, 353–370.

Suslov, S. A. 1997 Nonlinear analysis of non-Boussinesq convection. PhD thesis, University of Notre Dame, USA.

Suslov, S. A. & Paolucci, S. 1995*a* Stability of natural convection flow in a tall vertical enclosure under non-Boussinesq conditions. *Intl J. Heat Mass Transfer* **38**, 2143–2157.

Suslov, S. A. & Paolucci, S. 1995*b* Stability of mixed-convection flow in a tall vertical channel under non-Boussinesq conditions. *J. Fluid Mech.* **302**, 91–115.

Suslov, S. A. & Paolucci, S. 1997*a* Non-Boussinesq convection in a tall cavity near the codimension-2 point. *Proc. ASME Heat Transfer Division 3*. HTD-Vol. 353, pp. 243–250.

Suslov, S. A. & Paolucci, S. 1997*b* Nonlinear analysis of convection flow in a tall vertical enclosure under non-Boussinesq conditions. *J. Fluid Mech.* **344**, 1–41.

Suslov, S. A. & Paolucci, S. 1999 Nonlinear stability of mixed convection flow under non-Boussinesq conditions. Part 1. Analysis and bifurcations. *J. Fluid Mech.* **398**, 61–85.

Watson, J. 1960 On the non-linear mechanics of wave disturbances in stable and unstable parallel flows. Part 2. The development of a solution for plane Poiseuille flow and for plane Couette flow. *J. Fluid Mech.* **9**, 371–389.